International Journal of Solids and Structures 120 (2017) 199–212

Contents lists available at ScienceDirect

International Journal of Solids and Structures

journal homepage: www.elsevier.com/locate/ijsolstr

Analytical solutions for predicting tensile and in-plane shear strengths of triaxial weave fabric composites

J.B. Bai [a], J.J. Xiong [a,*], R.A. Shenoi [b], Y.T. Zhu [a]

[a] School of Transportation Science and Engineering, Beihang University, Beijing, 100191, People's Republic of China
[b] Southampton Marine and Maritime Institute, University of Southampton, Southampton, UK

ARTICLE INFO

Article history:
Received 19 January 2016
Revised 24 May 2016
Available online 2 May 2017

Keywords:
Composite
Triaxial weave fabric (TWF)
Strength
Tensile
In-plane shear

ABSTRACT

This paper deals with new analytical solutions to predict tensile and in-plane shear strengths of triaxial weave fabric (TWF) composites accounting for the interaction between angularly interlacing yarns. The triaxial yarns in three directions of 0° and ±60° in micromechanical unit cell (UC) are idealized as the curved beams with a path depicted by using sinusoidal shape functions. The tensile and in-plane shear strengths of TWF composites are derived by means of the minimum total complementary potential energy principle founded on micromechanics. In order to validate the new model, the predictions are compared with experimental data in prior literatures. It is shown that the predictions from the new model agree well with experimental results.

1. Introduction

Due to the superior specific stiffness and strength as well as excellent damage resistance and processing property, textile composites are undergoing a wide research and application in engineering structures (especially in aerospace structures) (Callus et al., 1999; Cheng and Xiong, 2009; Xiong et al., 2009; Mahadik and Hallett, 2011; Cheng et al., 2012; Bakar et al., 2013). Recently, with potential for the wider applications of triaxial weave fabric (TWF) composite structures (here the TWF means the net form with cavities between yarns), there is growing interest in assessing mechanical properties and failure mechanism for TWF composites using experimental, theoretical and numerical methods. Aoki et al. experimentally determined tensile stiffness and strength (Aoki and Yoshida, 2006), flexural stiffness (Aoki et al., 2007) and fatigue strength (Kosugi et al., 2011) of TWF composites. The experiments showed that tensile and flexural stiffness of TWF composites increased with the increasing width of specimen and eventually converged to a certain value. Fatigue strengths of TWF composites with thinner and thicker tows were almost same and fatigue failure progression of TWF composites with thicker tows was much slower as against that with thinner tows. Fatigue damage accumulation mechanism was attributed to the debonding at the tow intersection. Montesano et al. (2014) observed three main damage modes (including cracks within ±60° yarns, in resin rich zones and on yarn interfaces) and the changes of dominant cracks and crack density with stress level until final failure, by tracking the development of microscopic damage of TWF composites under axial tensile through scanning electron microscopes. Due to the resource constraints, various analytical models have been achieved to evaluate mechanical properties of TWF composites. Kueh et al. (2005), Kuth and Pellegrino (2007), and Kuth (2014) presented a transverse isotropic straight beam model to predict linear elastic response of TWF composites based on Kirchhoff plate theory. The tension, compression and shear properties were obtained by using the equivalent stiffness matrix determined from the FE method. The size effects on mechanical properties of TWF composites subjected to tensile and bending loadings were discussed. The predictions were in a good agreement with experimental data. Miravete et al. (2006) proposed an analytical meso-mechanical approach for predicting tensile modulus and strengths of TWF composites by considering the geometry, mechanical properties and the degradation of fiber and matrix. The new model was validated with numerical results and experimental data. Xu et al. (2007) developed an analytical method by using equivalent anisotropic plate theory to assess the buckling behavior of TWF composites subjected to a bi-axial compression loading. It was found that the buckling load increased with the increasing number of crossovers in TWF composites to approach a certain value. Predictions had a good correlation with the FE results. El-Hajjar et al. (2013) established discrete yarn and three-layer analytical models to evaluate the effects of braiding parameters on overall stiffness of TWF composites. Comparison between predictions and experiments showed the calculations from three-layer analytical model with the best prediction

* Corresponding author.
E-mail address: jjxiong@buaa.edu.cn (J.J. Xiong).

http://dx.doi.org/10.1016/j.ijsolstr.2017.05.002
0020-7683/

Nomenclature

A	cross-section area of yarns, mm^2
b	length of rhombic interlacing interface between triaxial yarns, mm
B_i	transformation variable
C_i	transformation variable
E	elastic modulus of yarn in longitudinal direction, MPa
F_1	equivalent external force on 0° yarn, N
F_{1f}	critical equivalent external force on 0° yarn pertinent to interlaminar shear failure of interlacing interface between triaxial yarns, N
F_2	equivalent external forces on ±60° yarns, N
G	in-plane shear modulus of yarn, MPa
h	thickness of yarn, mm
I_y	inertia moment of yarn along transverse direction, mm^4
I_z	inertia moment of yarn along through-thickness direction, mm^4
I_p	polar inertia moment of yarn, mm^4
J_i	transformation variable
K_i	transformation variable
L_0	length of the UC, mm
L	half undulation length of yarn, mm
M	internal bending moment, N · mm
M_1	internal bending moment on 0° yarn, N · mm
M_2	internal bending moment on ±60° yarns, N · mm
N	internal interaction force at the centre of interlacing interface between triaxial yarns along through-thickness direction, N
N_1	internal interactive force at the intersecting points between triaxial yarns along through-thickness direction, N
N_2	restraining force from yarn's rotation along through-thickness direction at the intersecting points between triaxial yarns, N
N_3	restraining force from yarn's rotation along through-thickness direction at the intersecting points between triaxial yarns, N
P_t	external uniaxial tensile force, N
P_{tf}	critical external uniaxial tensile force pertaining to tensile failure of TWF composites, N
P_{tf1}	critical external uniaxial tensile force pertaining to tensile failure of 0° yarn, N
P_{tf2}	critical external uniaxial tensile force pertaining to tensile failure of ±60° yarn, N
P_{S1}	external in-plane shear force along longitudinal direction, N
P_{S2}	external in-plane shear force along transverse direction, N
Q_i	transformation variable
S_0	interlaminar shear strength of yarn, MPa
S	in-plane shear strength per unit length of TWF composites, N/mm
T_1	internal torque moment on 0° yarn, N · mm
T_2	internal torque moment on ±60° yarn, N · mm
T_3	internal torque moment on interlacing interface between triaxial yarns resulted from restraining forces of N_2 and N_3, N · mm
U_1^*	complementary potential energy of 0° yarn in the UC
U_2^*	complementary potential energy of ±60° yarn in the UC
w	width of yarn, mm
W_0	width of the UC
W_p	torsional section modulus of interlacing interface between triaxial yarns, mm^3
X_{t0}	tensile strength of yarn in longitudinal direction, MPa
X_t	tensile strength per unit length of TWF composites, N/mm
σ_1	normal stress on 0° yarn, MPa
σ_2	normal stress on ±60° yarn, MPa
σ_t	tension force per unit length on the UC, N/mm
τ	interlaminar shear stress on interlacing interface between triaxial yarns, MPa
τ_1	shear force per unit length in longitudinal direction, N/mm
τ_2	shear force per unit length in transverse direction, N/mm
θ	off-axial angle of yarn, rad
Δ_{P_t}	relative shift of the UC in the direction of external force P_t, mm
$\Delta_{P_{S_1}}$	relative shift of the UC in the direction of external shear force P_{S1}, mm
ε	tension strain of the UC
γ	shear strain of the UC
FE	finite element
UC	unit cell
TWF	triaxial weave fabric

accuracy. Kuth (2013) presented a thin plate model to analyze the stability of sandwich columns with elastic cores of TWF composite skin-sheets subjected to uniaxial compression loading under simply support boundary condition. The effects of thickness, aspect ratio, modulus of core and imperfections in TWF composite skin-sheets on critical buckling loads were discussed. In recent years, the FE technique has also received considerable attention in assessing mechanical properties and failure mechanism of TWF composites. Zhao et al. (2004) simulated progressive failure process of TWF composites subjected to axial tensile loading in terms of the FE model and maximum stress, Hoffman and Tsai-Wu failure criterions. The numerical results coincided well with experiments. Aoki and Yoshida (2006) and Aoki et al. (2007) implemented a homogenization method based on the FE analysis of the UC to predict the in-plane flexural stiffness and the thermal expansion coefficient of TWF composites with the finite width under free boundary condition. Predictions had a good correlation with experiments. Tsai et al. (2008) developed a parallelogram spring model to investigate the effects of fabric parameters on elastic properties of TWF composites. Alternatively, fiber yarns were treated as a series of curved springs only with axial rigidity and the UC of braided composites was then discretized into the FE model with spring and solid elements under proper displacement boundary conditions. The predictions correlated well with theoretical results and experiments from previous literature. Zhang and Binienda (2014) numerically investigated mechanical behaviors of TWF composites with infinite size under both axial and transverse tensile loading by using a meso-scale FE model. The free-edge effects on global stress-strain response were simulated and local failure mechanisms were discussed. The numerical results coincided well with experiments. However, in order to produce the FE models, straight inclined segments or continuous mathematical functions have been used to depict in more detail the idealized TWF geometry including yarn path and cross-sectional shape. The one draw back of the FE models is their intensity and complexity. It is obvious that the analytical methods still have consistently received interests to evaluate

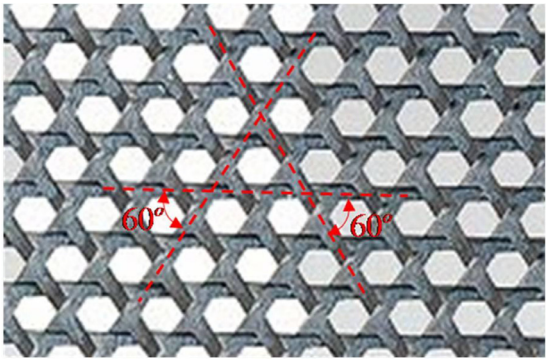

Fig. 1. TWF composites (Miravete et al., 2006).

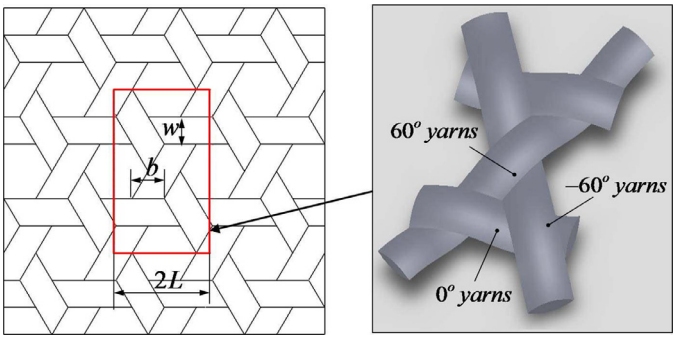

Fig. 2. Representative unit cell of TWF composites.

mechanical properties of textile composites and there is a need for a more practical and expedient analytical model for structural applications, especially in aerospace field.

In this paper, an attempt is made to develop novel analytical models to predict tensile and in-plane shear strengths of TWF composites by using the minimum total complementary potential energy principle based on apt geometrical approximation and assumptions for TWF composites. New analytical solutions for predicting tensile and in-plane shear strengths are established. The results from the models are compared with experimental data from the prior literatures.

2. Geometrical model for TWF composites

It is well known that quasi-isotropic macro-mechanical behaviors of TWF composites depend upon fabric geometry (e.g., cross-section and undulation geometry of yarn), fiber volume fraction and constituent properties, etc. In general, the TWF composites are formed by angularly interlacing and curing the preformed yarns in the directions of 0° and ±60° (shown in Fig. 1), and the crimp or undulation of yarns resulted from the angularly interlacing between triaxial yarns has a significant influence on mechanical properties and strengths of TWF composites. The periodicity of the repeating pattern in a TWF can be used to isolate a small UC (unit cell) which is sufficient to describe the fabric architecture. The UC in yarn interlacing pattern for a TWF is indicated in Fig. 2 by dark borders. From Fig. 2, it is clear that the undulated length of 0° yarn is twice those of ±60° yarns in the UC, and it can be shown that

$$L_0 = \frac{2L}{\tan 30^\circ} = 2L\sqrt{3} \tag{1}$$

$$W_0 = 2L \tag{2}$$

where L_0 and W_0 are respectively the length and width of the UC. L is the half undulated length of 0° yarn.

Fig. 3 shows the micrograph of 0° yarn obtained from scanning electron microscopes and illustrates the definitions of three directions of x y and z axis in local coordinate system. The coordinate axes x y and z respectively denote the longitudinal, transverse and through-thickness directions of the yarns to ensure the fibers with correct 3D orientation, i.e., to keep three directions of x, y and z axis in local coordinate system consistent with three normal stresses. In order to establish analytical models of the UC, fundamental assumptions made in this paper are as follows:

(1) The yarns are idealized as the curved beams with an undulated neutral axis depicted by using a smooth and continuous sinusoidal curve function (shown in Fig. 3).
(2) The flat cross-section of yarns is regarded as the rectangular section with the width of w and the thickness of h (shown in Fig. 4).
(3) The interlacing interface between triaxial yarns is approximated as the rhombus section with the width of w and the length of b (shown in Fig. 5).
(4) Previous literatures (Aoki and Yoshida, 2006; Kuth and Pellegrino, 2007) show that the load-strain response for TWF composites under uniaxial tensile state was linear until final brittle rupture and no obvious yield took place (see Fig. 6), whereas the load-strain response under in-plane shear state had the linear elastic and nonlinear regions until final failure, but the yield strength was close to the ultimate strength (see Fig. 7). Therefore, the failure strength in this work is defined as the critical stress at failure initiation (i.e., at initial load drop on the load-displacement response) before the decrease of modulus, and the decrease of modulus is neglected.
(5) Shear force component is negligibly small in contrast to the axial force in tensile or compression case for plane woven composites, while the axial force component is negligibly small in comparison with the shear force in pure shear loading case (Potluri and Thammandra, 2007; Naik et al., 2003).

From Assumption (1) and Fig. 3, the undulated neutral axis of triaxial yarns can be expressed by a sinusoidal function.

$$z = \frac{h}{2}\sin\frac{\pi x}{L} \tag{3}$$

where h is the thickness of yarn.

From Assumption (2) and Fig. 4, the area and inertia moments of idealized cross-section of triaxial yarns are respectively

$$A = wh \tag{4}$$

$$I_y = \frac{wh^3}{12} \tag{5}$$

$$I_z = \frac{w^3h}{12} \tag{6}$$

$$I_p = I_y + I_z \tag{7}$$

where A is cross-section area of yarn. I_y and I_z are respectively the inertia moment of yarn along transverse and through-thickness directions of yarn. I_p is the polar inertia moment.

From Assumption (3) and Fig. 5, the torsional section modulus of rhombic interlacing interface between triaxial yarns can be written as

$$W_p = \alpha w b^2 \tag{8}$$

with

$$b = \frac{w}{\cos 30^\circ} = \frac{2w\sqrt{3}}{3} \tag{9}$$

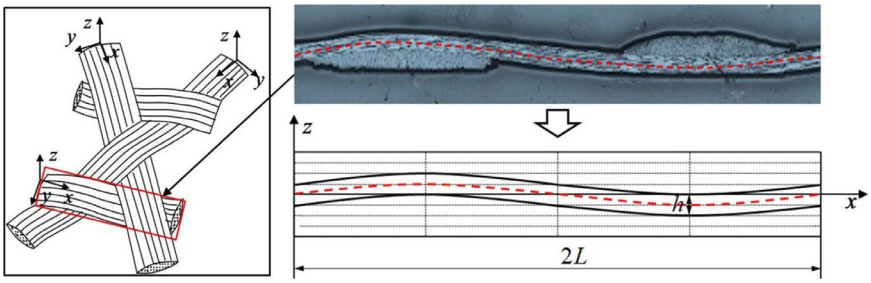

Fig. 3. Local coordinate systems and idealized geometric configuration of 0° yarn.

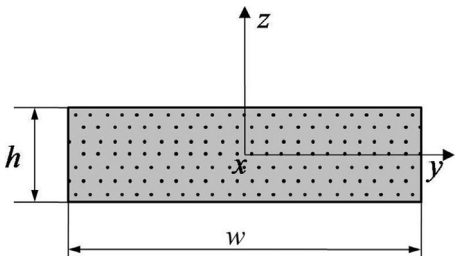

Fig. 4. Idealized cross-section for triaxial yarns.

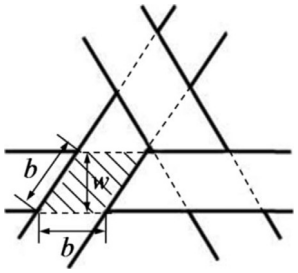

Fig. 5. Idealized interlacing interface between triaxial yarns.

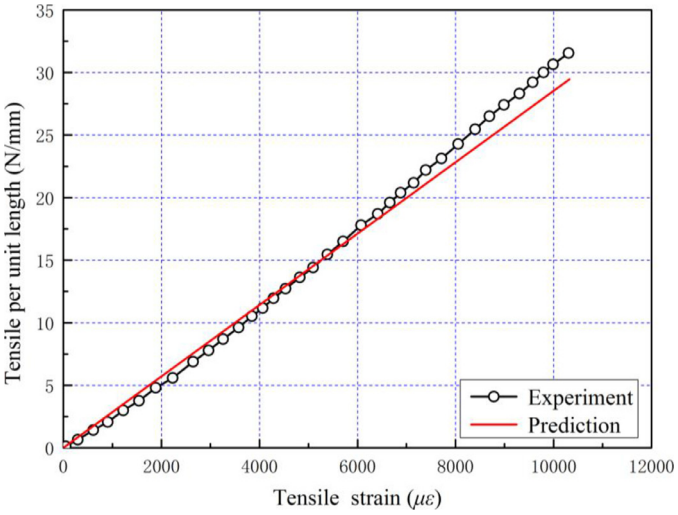

Fig. 6. Tensile force per unit length versus strain curve (Aoki and Yoshida, 2006).

where W_p is the torsional section modulus. w is the width of yarn. b is the length of rhombic interlacing interface between triaxial yarns. α is the correct coefficient, for the rhombus section, $\alpha = 0.1181$.

Substituting Eq. (9) into Eq. (8) deduces

$$W_p = \frac{4}{3}\alpha w^3 \tag{10}$$

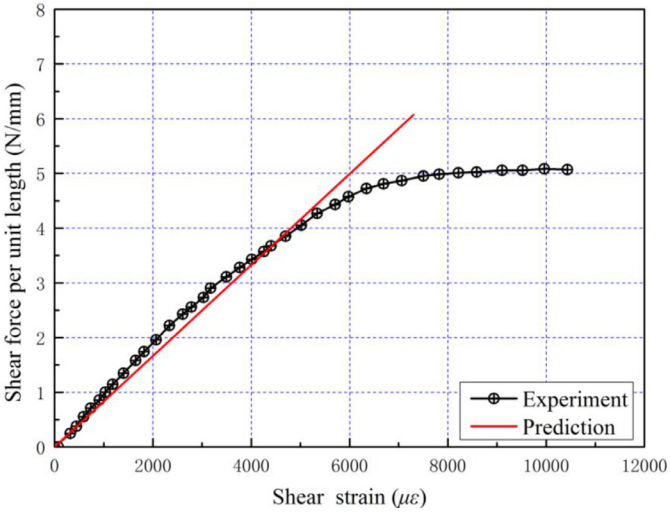

Fig. 7. Shear force per unit length versus strain curve (Kuth and Pellegrino, 2007).

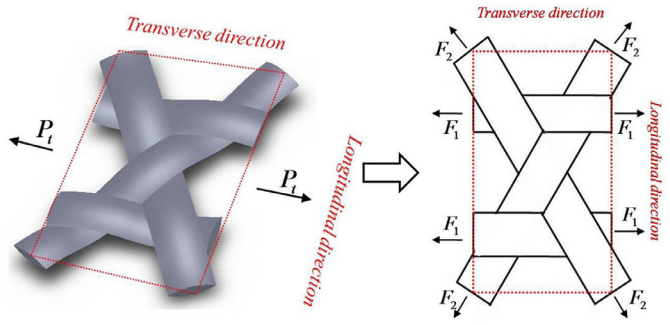

Fig. 8. External uniaxial tensile force and equivalent external forces on triaxial yarns.

3. Analytical solution for tensile strength

As shown in Fig. 8, in the case of external uniaxial tensile loading P_t, there are equivalent external axial forces F_1 and F_2 on 0° and ±60° yarns in the UC. In order to obtain the equivalent external axial forces F_1 and F_2 on 0° and ±60° yarns, with the aid of force decomposition as a vector, it is possible to have

$$P_t = 2F_1 + 2F_2 \sin 30^\circ \tag{11}$$

or

$$F_2 = P_t - 2F_1 \tag{12}$$

where P_t is the external uniaxial tensile force. F_1 and F_2 are respectively the equivalent external axial forces on 0° and ±60° yarns.

Due to the rotationally symmetry of the UC, only half UC necessitates to be analyzed. Figs. 9a and b respectively illustrate the

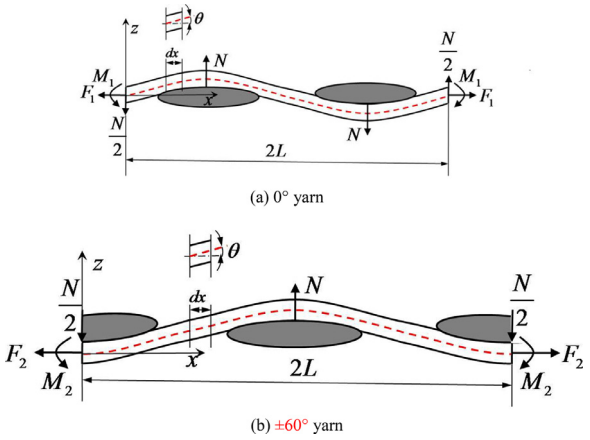

Fig. 9. Internal forces and bending moments on 0° and ±60° yarns in uniaxial tensile state.

internal force and bending moments on 0° and ±60° yarns (where N is the internal interaction force at the centre of interlacing interface between triaxial yarns along through-thickness direction. M_1 and M_2 respectively represent the internal bending moments on 0° and ±60° yarns). In terms of moment equilibrium of half UC, one has

$$M_1 = 0 \tag{13}$$

From Fig. 9a, for a differential segment dx on 0° yarn, by means of Eq. (3), the tangent of off-axial angle can be shown to be

$$\tan\theta = \frac{dz}{dx} = \frac{\pi h}{2L}\cos\left(\frac{\pi}{L}x\right) \tag{14}$$

where θ is the off-axial angle of yarn.

The internal force and bending moment on any cross-section of 0° yarn can be expressed as

$$F(x) = F_1\cos\theta = \frac{F_1}{\sqrt{1+\tan^2\theta}} \qquad \left(0 \le x \le \tfrac{L}{2}\right) \tag{15}$$

$$M(x) = \frac{hF_1}{2}\sin\frac{\pi x}{L} - \frac{N}{2}x \qquad \left(0 \le x \le \tfrac{L}{2}\right) \tag{16}$$

Substituting Eq. (14) into Eq. (15) results in

$$F(x) = \frac{F_1}{\sqrt{1+\left(\frac{\pi h}{2L}\cos\frac{\pi x}{L}\right)^2}} \qquad \left(0 \le x \le \tfrac{L}{2}\right) \tag{17}$$

By analogy aid of Eqs. (16) and (17), it is possible to have the internal force and bending moment on any cross-section of ±60° yarn as

$$F(x) = \frac{P_t - 2F_1}{\sqrt{1+\left(\frac{\pi h}{2L}\sin\frac{\pi x}{L}\right)^2}} \qquad (0 \le x \le L) \tag{18}$$

$$M(x) = \left(\frac{P_t}{2} - F_1\right)\left(1-\cos\frac{\pi x}{L}\right)h - \frac{N}{2}x - M_2 \qquad (0 \le x \le L) \tag{19}$$

It goes without saying that there exist three undetermined forces and moments of F_1, N and M_2 in Eqs. (16)–(19), and it is feasible to determine these undetermined forces and moments in view of the principle of minimum total complementary potential energy. The complementary potential energies of 0° and ±60° yarns in the UC are respectively

$$U_1^* = \frac{2}{EI_y}\int_0^{\frac{L}{2}} M^2(x)\sqrt{1+\left(\frac{\pi h}{2L}\cos\frac{\pi x}{L}\right)^2}\,dx + \frac{2}{EA}\int_0^{\frac{L}{2}} F^2(x)\sqrt{1+\left(\frac{\pi h}{2L}\cos\frac{\pi x}{L}\right)^2}\,dx \tag{20}$$

$$U_2^* = \frac{1}{EI_y}\int_0^{L} M^2(x)\sqrt{1+\left(\frac{\pi h}{2L}\sin\frac{\pi x}{L}\right)^2}\,dx + \frac{1}{EA}\int_0^{L} F^2(x)\sqrt{1+\left(\frac{\pi h}{2L}\sin\frac{\pi x}{L}\right)^2}\,dx \tag{21}$$

where U_1^* and U_2^* are respectively the complementary potential energies of 0° and ±60° yarns in the UC. E is the elastic modulus of yarn in longitudinal direction. Note that the square root factors in Eqs. (20) and (21) are the transformation coefficients for infinitesimal element length dx mapped to the neutral axis of curved beam.

Substituting Eqs. (16)–(19) into Eqs. (20) and (21), it can be shown that

$$U_1^* = (B_1+B_4)F_1^2 + B_2N^2 + B_3F_1N \tag{22}$$

$$U_2^* = (B_5+B_{11})\left(\frac{P_t}{2}-F_1\right)^2 + B_6N^2 + B_7M_2^2 + B_8N\left(\frac{P_t}{2}-F_1\right) + B_9M_2\left(\frac{P_t}{2}-F_1\right) + B_{10}NM_2 \tag{23}$$

where B_i (i=1, 2, ⋯, 11) are the transformation variables and are defined in Appendix A.

Because the complementary potential energies of −60° and 60° yarns are same, from Eqs. (22) and (23), total complementary potential energy of the UC can be shown to be

$$\Pi^* = 2U_1^* + 4U_2^* = 2(B_1+B_4)F_1^2 + 4(B_5+B_{11})\left(\frac{P_t}{2}-F_1\right)^2 + (2B_2+4B_6)N^2 + 4B_7M_2^2 + 2B_3F_1N + 4B_8N\left(\frac{P_t}{2}-F_1\right) + 4B_9M_2\left(\frac{P_t}{2}-F_1\right) + 4B_{10}NM_2 \tag{24}$$

By minimizing the total complementary potential energy principle of the UC and taking transformation leads to

$$\begin{cases} [2(B_1+B_4)+4(B_5+B_{11})]F_1 + (B_3-2B_8)N - 2B_9M_2 = 2(B_5+B_{11})P_t \\ (B_3-2B_8)F_1 + 2(B_2+2B_6)N + 2B_{10}M_2 = -B_8P_t \\ -2B_9F_1 + 2B_{10}N + 4B_7M_2 = -B_9P_t \end{cases} \tag{25}$$

Solving Eq. (25) by using Cramer's rule shows

$$F_1 = C_1P_t \tag{26}$$

$$N = C_2P_t \tag{27}$$

$$M_2 = C_3P_t \tag{28}$$

where C_i (i=1, 2, 3) are the transformation variables and are defined in Appendix B.

With the aid of the potential energy principle, the relative shift Δ_{P_t} of the UC in the direction of external force P_t is deduced as

$$\Delta_{P_t} = \frac{\partial\Pi^*}{\partial P_t} = 4(B_1+B_4)C_1^2P_t + 8(B_5+B_{11})(0.5-C_1)^2P_t + 4(B_2+2B_6)C_2^2P_t + 8B_7C_3^2P_t + 4B_3C_1C_2P_t + 8B_8C_2(0.5-C_1)P_t + 8B_9C_3(0.5-C_1)P_t + 8B_{10}C_2C_3P_t \tag{29}$$

In light of the definition of strain, tension strain ε of the UC is

$$\varepsilon = \frac{\Delta_{P_t}}{2L} \tag{30}$$

And the tension force per unit length on the UC is determined as

$$\sigma_t = \frac{P_t}{2\sqrt{3}L} \tag{31}$$

On the basis of engineering beam theory, maximum normal stresses at the path peaks and valleys of 0° and ±60° yarns in the UC resulted from internal force and bending moment can be respectively written as

$$\sigma_{1\max} = \frac{F_1}{A} + \frac{NLh}{8I_y} \tag{32}$$

$$\sigma_{2\max} = \frac{F_2}{A} + \frac{NLh + 2M_2h}{4I_y} \tag{33}$$

where σ_1 and σ_2 are respectively the normal stresses on 0° and ±60° yarns.

Substituting Eqs. (12), (26)–(28) into Eqs. (32) and (33) yields

$$\sigma_{1\,\max} = P_t\left(\frac{C_1}{A} + \frac{C_2Lh}{8I_y}\right) \tag{34}$$

$$\sigma_{2\,\max} = P_t\left(\frac{1-2C_1}{A} + \frac{C_2L+2C_3}{4I_y}h\right) \tag{35}$$

According to the maximum stress criterion, from Eqs. (34) and (35), critical external uniaxial tensile forces pertaining to tensile failures of 0° and ±60° yarns are respectively

$$P_{tf1} = X_{t0}\left(\frac{C_1}{A} + \frac{C_2Lh}{8I_y}\right)^{-1} \tag{36}$$

$$P_{tf2} = X_{t0}\left(\frac{1-2C_1}{A} + \frac{C_2L+2C_3}{4I_y}h\right)^{-1} \tag{37}$$

where P_{tf1} and P_{tf2} are respectively the critical external uniaxial tensile forces pertaining to tensile failures of 0° and ±60° yarns. X_{t0} is the tensile strength of yarn in longitudinal direction.

From Eqs. (36) and (37), critical external uniaxial tensile force pertaining to tensile failure of TWF composites is obtained as

$$P_{tf} = \min\left(P_{tf1}, P_{tf2}\right) \tag{38}$$

where P_{tf} is the critical external uniaxial tensile force pertinent to tensile failure of TWF composites.

From Eqs. (1) and (38), the tensile strength per unit length of TWF composites is attained as

$$X_t = \frac{P_{tf}}{L_0} = \frac{\min\left(P_{tf1}, P_{tf2}\right)}{2L\sqrt{3}} \tag{39}$$

where X_t is the tensile strength per unit length of TWF composites.

4. Analytical solution for in-plane shear strength

From Fig. 10, it is clear that for the UC of TWF composites subjected to external in-plane shear loading of P_{S1} and P_{S2}, there exist equivalent external shear forces F_1 and F_2 on 0° and ±60° yarns. Similarly, with the aid of force decomposition, it is possible to have

$$P_{S1} = 2F_1 - 2F_2\sin 30^\circ \tag{40}$$

$$P_{S2} = 2F_2\cos 30^\circ \tag{41}$$

where P_{S1} and P_{S2} are respectively the external in-plane shear forces along longitudinal and transverse directions.

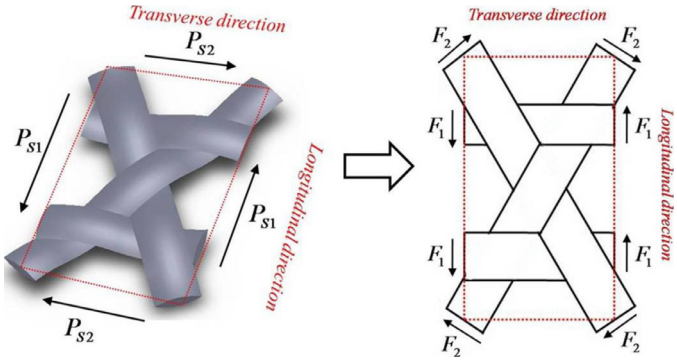

Fig. 10. External in-plane shear forces and equivalent external forces on triaxial yarns.

According to moment equivalence of the UC, one has

$$F_1 = 2F_2 \tag{42}$$

Substituting Eq. (42) into Eqs. (40) and (41) yields

$$F_1 = \frac{2}{3}P_{S_1} \tag{43}$$

From Eqs. (1) and (2), the in-plane shear forces per unit length on the UC in longitudinal and transverse directions are respectively

$$\tau_1 = \frac{P_{S1}}{L_0} = \frac{P_{S1}}{2\sqrt{3}L} \tag{44}$$

$$\tau_2 = \frac{P_{S2}}{W_0} = \frac{P_{S2}}{2L} \tag{45}$$

where τ_1 and τ_2 respectively denote the in-plane shear forces per unit length on the UC in longitudinal and transverse directions.

Substituting Eqs. (40)–(42) into Eqs. (44) and (45) results in

$$\tau_1 = \frac{F_2\sqrt{3}}{2L} \tag{46}$$

$$\tau_2 = \frac{F_2\sqrt{3}}{2L} \tag{47}$$

From Eqs. (46) and (47), it is clear that the in-plane shear force per unit length on the UC in longitudinal direction is equal to that in transverse direction. This implies that the micro-mechanical curved beam model of yarns in the UC follows the equivalent law of shear stress.

Figs. 11a and b respectively demonstrate the internal restraining forces and moments on 0° and 60° yarns (where N_1 is the internal interactive force at the intersecting points between triaxial yarns along through-thickness direction. N_2 and N_3 are the restraining forces from yarn's rotation along through-thickness direction at the intersecting points between triaxial yarns to depict the shearing action at the interlace area. T_1, T_2, M_1 and M_2 are respectively the internal torque and bending moments on 0° and 60° yarns). From Fig. 11a, it is possible to have the internal bending and torque moments at any cross-section of 0° yarn as

$$M_y(x) = \begin{cases} N_1x - \frac{N_3h}{4}\sin\frac{\pi x}{L} & \left(0 \le x < \frac{L}{3}\right) \\ \frac{N_1L}{3} - \frac{N_3h}{4}\sin\frac{\pi x}{L} + \frac{N_2h\sqrt{3}}{8}\left(2\sin\frac{\pi x}{L} - \sqrt{3}\right) & \left(\frac{L}{3} \le x < \frac{L}{2}\right) \end{cases} \tag{48}$$

$$M_z(x) = \begin{cases} M_1 - F_1x + \frac{N_3x\sqrt{3}}{2} & \left(0 \le x < \frac{L}{3}\right) \\ M_1 - F_1x + \frac{N_3}{4}\left(2x\sqrt{3} + b\right) & \\ \quad + \frac{N_2}{4}\left(2x + b\sqrt{3}\right) & \left(\frac{L}{3} \le x < \frac{L}{2}\right) \end{cases} \tag{49}$$

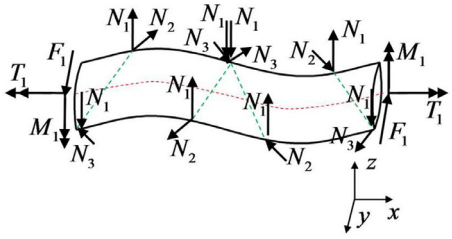

(a) 0° yarn

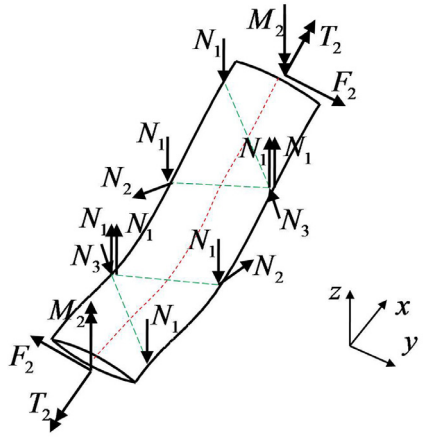

(b) ±60° yarn

Fig. 11. Internal forces and moments on 0° and 60° yarns under in-plane shear condition (Note that the green dotted lines represent the interlacing edges between triaxial yarns).

$$T(x)=\begin{cases} T_1+\frac{F_1h}{2}\sin\frac{\pi x}{L}-\frac{N_1b}{2} & \\ \quad -\frac{N_3h\sqrt{3}}{4}\sin\frac{\pi x}{L} & \left(0\le x<\frac{L}{3}\right)\\ T_1+\frac{F_1h}{2}\sin\frac{\pi x}{L}-N_1b & \\ \quad -\frac{N_3h\sqrt{3}}{4}\sin\frac{\pi x}{L} & \\ \quad -\frac{N_2h}{8}\left(2\sin\frac{\pi x}{L}-\sqrt{3}\right) & \left(\frac{L}{3}\le x<\frac{L}{2}\right)\end{cases} \tag{50}$$

Using Eqs. (48)–(50) as an analogy, from Fig. 11b, the internal bending and torque moments at any cross-section of 60° yarn are obtained as

$$M_y(x)=\begin{cases} 0 & \left(0\le x<\frac{L}{6}\right)\\ -N_1\left(x-\frac{L}{6}\right) & \left(\frac{L}{6}\le x<\frac{L}{2}\right)\\ \frac{N_1}{6}(6x-5L)+\frac{N_3h}{4}\cos\frac{\pi x}{L} & \left(\frac{L}{2}\le x<\frac{5L}{6}\right)\\ \frac{N_3h}{4}\cos\frac{\pi x}{L}+\frac{N_2h\sqrt{3}}{8}\left(\sqrt{3}-2\cos\frac{\pi x}{L}\right) & \left(\frac{5L}{6}\le x<L\right)\end{cases} \tag{51}$$

$$M_z(x)=\begin{cases} M_2-F_2x & \left(0\le x<\frac{L}{2}\right)\\ M_2-F_2x+\frac{N_3}{4}\left(2x\sqrt{3}+b-L\sqrt{3}\right) & \left(\frac{L}{2}\le x<\frac{5L}{6}\right)\\ M_2-F_2x+\frac{N_3}{4}\left(2x\sqrt{3}+b-L\sqrt{3}\right) & \\ \quad +\frac{N_2}{12}\left(6x+3b\sqrt{3}-5L\right) & \left(\frac{5L}{6}\le x<L\right)\end{cases} \tag{52}$$

$$T(x)=\begin{cases} T_2+\frac{F_2h}{2}\left(1-\cos\frac{\pi x}{L}\right) & \left(0\le x<\frac{L}{6}\right)\\ T_2+\frac{F_2h}{2}\left(1-\cos\frac{\pi x}{L}\right)-\frac{N_1b}{2} & \left(\frac{L}{6}\le x<\frac{L}{2}\right)\\ T_2+\frac{F_2h}{2}\left(1-\cos\frac{\pi x}{L}\right)-\frac{3N_1b}{2} & \\ \quad +\frac{N_3h\sqrt{3}}{4}\cos\frac{\pi x}{L} & \left(\frac{L}{2}\le x<\frac{5L}{6}\right)\\ T_2+\frac{F_2h}{2}\left(1-\cos\frac{\pi x}{L}\right)-2N_1b & \\ \quad +\frac{N_3h\sqrt{3}}{4}\cos\frac{\pi x}{L} & \\ \quad -\frac{N_2h}{8}\left(\sqrt{3}-2\cos\frac{\pi x}{L}\right) & \left(\frac{5L}{6}\le x<L\right)\end{cases} \tag{53}$$

It stands to reason that there are seven undetermined forces and moments N_1, N_2, N_3, M_1, M_2, T_1 and T_2 in Eqs. (48)–(53). Using the same method as in the above section, these undetermined forces and moments can be determined by resorting to the principle of minimum complementary energy. The complementary potential energies of 0° and 60° yarns in the UC are respectively

$$\begin{aligned} U_1^*=&\frac{2}{EI_y}\int_0^{\frac{L}{2}}M_y^2(x)\sqrt{1+\left(\frac{\pi h}{2L}\cos\frac{\pi x}{L}\right)^2}dx\\ &+\frac{2}{EI_z}\int_0^{\frac{L}{2}}M_z^2(x)\sqrt{1+\left(\frac{\pi h}{2L}\cos\frac{\pi x}{L}\right)^2}dx\\ &+\frac{2}{GI_p}\int_0^{\frac{L}{2}}T^2(x)\sqrt{1+\left(\frac{\pi h}{2L}\cos\frac{\pi x}{L}\right)^2}dx \end{aligned} \tag{54}$$

$$\begin{aligned} U_2^*=&\frac{1}{EI_y}\int_0^{L}M_y^2(x)\sqrt{1+\left(\frac{\pi h}{2L}\sin\frac{\pi x}{L}\right)^2}dx\\ &+\frac{1}{EI_z}\int_0^{L}M_z^2(x)\sqrt{1+\left(\frac{\pi h}{2L}\sin\frac{\pi x}{L}\right)^2}dx\\ &+\frac{1}{GI_p}\int_0^{L}T^2(x)\sqrt{1+\left(\frac{\pi h}{2L}\sin\frac{\pi x}{L}\right)^2}dx \end{aligned} \tag{55}$$

where G is the in-plane shear modulus of yarn.

Substituting Eqs. (48)–(53) into Eqs. (54) and (55) leads to

$$\begin{aligned} U_1^*=&Q_1F_1^2+Q_2M_1^2+Q_3T_1^2+Q_4N_1^2+Q_5N_2^2+Q_6N_3^2+Q_7F_1M_1\\ &+Q_8F_1T_1+Q_9F_1N_1+Q_{10}F_1N_2+Q_{11}F_1N_3+Q_{12}M_1N_2\\ &+Q_{13}M_1N_3+Q_{14}T_1N_1+Q_{15}T_1N_2+Q_{16}T_1N_3+Q_{17}N_1N_2\\ &+Q_{18}N_1N_3+Q_{19}N_2N_3 \end{aligned} \tag{56}$$

$$\begin{aligned} U_2^*=&Q_{20}F_2^2+Q_{21}M_2^2+Q_{22}T_2^2+Q_{23}N_1^2+Q_{24}N_2^2+Q_{25}N_3^2\\ &+Q_{26}F_2M_2+Q_{27}F_2T_2+Q_{28}F_2N_1+Q_{29}F_2N_2+Q_{30}F_2N_3\\ &+Q_{31}M_2N_2+Q_{32}M_2N_3+Q_{33}T_2N_1+Q_{34}T_2N_2+Q_{35}T_2N_3\\ &+Q_{36}N_1N_2+Q_{37}N_1N_3+Q_{38}N_2N_3 \end{aligned} \tag{57}$$

where $Q_i(i=1, 2.....38)$ are the transformation variables and are defined in Appendices C–E.

From Eqs. (56) and (57), total complementary potential energy of the UC becomes

$$\begin{aligned} \overset{*}{\prod}=&2Q_1F_1^2+2Q_2M_1^2+2Q_3T_1^2+4Q_{20}F_2^2+4Q_{21}M_2^2+4Q_{22}T_2^2\\ &+(2Q_4+4Q_{23})N_1^2+(2Q_5+4Q_{24})N_2^2+(2Q_6+4Q_{25})N_3^2\\ &+2Q_7F_1M_1+2Q_8F_1T_1\\ &+2Q_9F_1N_1+2Q_{10}F_1N_2+2Q_{11}F_1N_3+2Q_{12}M_1N_2\\ &+2Q_{13}M_1N_3+2Q_{14}T_1N_1+2Q_{15}T_1N_2+2Q_{16}T_1N_3\\ &+(2Q_{17}+4Q_{36})N_1N_2+(2Q_{18}+4Q_{37})N_1N_3\\ &+(2Q_{19}+4Q_{38})N_2N_3+4Q_{26}F_2M_2+4Q_{27}F_2T_2+4Q_{28}F_2N_1\\ &+4Q_{29}F_2N_2+4Q_{30}F_2N_3+4Q_{31}M_2N_2+4Q_{32}M_2N_3\\ &+4Q_{33}T_2N_1+4Q_{34}T_2N_2+4Q_{35}T_2N_3 \end{aligned} \tag{58}$$

By minimizing total complementary potential energy of the UC and taking transformation, it can be shown that

$$\begin{bmatrix} M_1 \\ T_1 \\ M_2 \\ T_2 \\ N_1 \\ N_2 \\ N_3 \end{bmatrix} = -F_1 \begin{bmatrix} 4Q_2 & 0 & 0 & 0 & 0 & 2Q_{12} & 2Q_{13} \\ 0 & 4Q_3 & 0 & 0 & 2Q_{14} & 2Q_{15} & 2Q_{16} \\ 0 & 0 & 8Q_{21} & 0 & 0 & 4Q_{31} & 4Q_{32} \\ 0 & 0 & 0 & 8Q_{22} & 4Q_{33} & 4Q_{34} & 4Q_{35} \\ 0 & 2Q_{14} & 0 & 4Q_{33} & 4(Q_4+2Q_{23}) & 2(Q_{17}+2Q_{36}) & 2(Q_{18}+2Q_{37}) \\ 2Q_{12} & 2Q_{15} & 4Q_{31} & 4Q_{34} & 2(Q_{17}+2Q_{36}) & 4(Q_5+2Q_{24}) & 2(Q_{19}+2Q_{38}) \\ 2Q_{13} & 2Q_{16} & 4Q_{32} & 4Q_{35} & 2(Q_{18}+2Q_{37}) & 2(Q_{19}+2Q_{38}) & 4(Q_6+2Q_{25}) \end{bmatrix}^{-1} \begin{bmatrix} 2Q_7 \\ 2Q_8 \\ 2Q_{26} \\ 2Q_{27} \\ 2(Q_9+Q_{28}) \\ 2(Q_{10}+Q_{29}) \\ 2(Q_{11}+Q_{30}) \end{bmatrix} \tag{59}$$

By numerically solving Eq. (59), one has

$$N_2 = C_4 F_1 \tag{60}$$

$$N_3 = C_5 F_1 \tag{61}$$

where C_4 and C_5 are the transformation variables.

Substituting Eq. (43) into Eq. (59), and then substituting Eq. (59) into Eq. (58), the total complementary potential energy of the UC can be expressed with the external shear loading P_{S1}. Again, using the same method as in the above section (or in accordance with the potential energy principle), the relative shift $\Delta_{P_{S1}}$ of the RUC in the direction of the external shear loading P_{S1} is determined as

$$\Delta_{P_{S1}} = \frac{\partial \prod^*}{\partial P_{S1}} \tag{62}$$

In interest of the definitions of shear strain, the shear strain γ of the TWF composites is

$$\gamma = \frac{\Delta_{P_{S1}}}{2L} \tag{63}$$

In reality, for the UC of TWF composites subjected to external in-plane shear loading, there exists an interlaminar shear stress on the interlacing interface between triaxial yarns and the shear debonding failure always occurs at the interlacing interface between triaxial yarns in TWF composites due to the lower interlaminar shear strength (Kosugi et al., 2011). Hereby, the in-plane shear properties and strength of TWF composites are dependent on the interlaminar shear strength of interlacing interface between triaxial yarns. From Fig. 11, the internal torsion moment on the interlacing interface between triaxial yarns along through-thickness direction resulted from the restraining forces N_2 and N_3 can be written as

$$T_3 = b\left(N_2 + N_3\sqrt{3}\right) \tag{64}$$

where T_3 is the internal torque moment on the interlacing interface between triaxial yarns resulted from restraining forces of N_2 and N_3.

Substituting Eqs. (60) and (61) into Eq. (64) results in

$$T_3 = bF_1\left(C_4 + C_5\sqrt{3}\right) \tag{65}$$

According to mechanics of materials, maximum interlaminar shear stress on the interlacing interface between triaxial yarns is determined as

$$\tau_{\max} = \frac{T_3}{W_p} \tag{66}$$

where τ is the interlaminar shear stress on interlacing interface between triaxial yarns.

Substituting Eqs. (10) and (65) into Eq. (66) leads to

$$\tau_{\max} = \frac{3bF_1}{4\alpha w^3}\left(C_4 + C_5\sqrt{3}\right) \tag{67}$$

According to the maximum stress criterion, from Eq. (67), critical equivalent external force on 0° yarn pertinent to interlaminar shear failure of interlacing interface between triaxial yarns can be shown to be

$$\frac{3bF_{1f}}{4\alpha w^3}\left(C_4 + C_5\sqrt{3}\right) = S_0 \tag{68}$$

namely,

$$F_{1f} = \frac{4S_0\alpha w^3}{3b\left(C_4 + C_5\sqrt{3}\right)} \tag{69}$$

where F_{1f} is the critical equivalent external force on 0° yarn pertinent to interlaminar shear failure of interlacing interface between triaxial yarns. S_0 is the interlaminar shear strength of yarn.

From Eqs. (43), (46) or (47) and (69), the in-plane shear strength per unit length of TWF composites becomes

$$S = \frac{\sqrt{3}}{4L}F_{1f} = \frac{\sqrt{3}\alpha S_0 w^3}{3bL\left(C_4 + C_5\sqrt{3}\right)} \tag{70}$$

where S is the in-plane shear strength per unit length of TWF composites.

5. Comparisons between predictions and experiments

In order to validate new analytical models presented in this paper, it is essential to compare the predictions determined from the new models with the experiments. Previous literatures reported the fabric specifications and mechanical properties (shown in Table 1) and the experiments of tensile and in-plane shear strengths (shown in Figs. 6 and 7 and Table 2) for three types of TWF composites (i.e., T300/NM35 (Aoki and Yoshida, 2006; Aoki et al., 2007), T300/Hexel 8552 (Kuth and Pellegrino, 2007; Zhao, 2010) and another carbon fiber/epoxy resin (Zhao et al., 2004)).

From the fabric specifications and mechanical properties listed in Table 1, by using Eqs. (30), (31), (39), (44), (63) and (70), the tensile and in-plane shear forces per unit length versus strain curves and the tensile and in-plane shear strengths of three types of TWF composites are respectively predicted (shown in Figs. 6 and 7, and Table 2). From Figs. 6 and 7, it is obvious that the predicting curves correlate very well with experiments in the linear elastic range before the decrease of modulus. From Table 2, it is evident that the maximum relative deviations of predictions for tensile and in-plane shear strengths from experiments are respectively 3.4% and 20.44%, with an acceptable scatter. The reason for 20.44% in the difference between the predicted and experimental values is probably that the predictions are obtained from Assumption (4) (namely, the decrease of modulus is neglected). However, the load-strain response under in-plane shear state had the linear elastic and nonlinear regions until final failure (see Fig. 7). This results in the predicted shear strengths in this work (i.e., at initial load drop on the shear load-displacement response before the decrease of modulus) being stiffer than those shown in the experimental ones.

From mentioned above, it is argued that the new curved beam-based models presented in this paper are a valid and rational basis for tensile and in-plane shear strength analysis of TWF composites. Using these models, tensile and in-plane shear strengths of TWF composites could be predicted without any additional fabric level experimental investigation, i.e. only the input of basic properties of

Table 1
Fabric specifications and mechanical properties of yarn.

	w/mm	h/mm	L/mm	E/MPa	G/MPa	X_{t0}/MPa	S_0/MPa
T300/Hexel8552 (Kuth and Pellegrino, 2007; Zhao, 2010)	0.803	0.078	1.56	153,085	4408	2296	92
T300/NM35 (Aoki and Yoshida, 2006; Aoki et al., 2007)	0.89	0.07	1.55	176,000	6860	2673	N.A.
Carbon fiber/epoxy resin (Zhao et al., 2004)	0.85	0.07	1.59	338,570	5610	3400	N.A.

Table 2
Tensile and shear strengths per unit length of TWF composites.

		T300/Hexel8552	T300/NM35	Carbon fiber/epoxy resin
X_t/N/mm	Experiments	25.85 (Kuth and Pellegrino, 2007; Zhao, 2010)	30.58 (Aoki and Yoshida, 2006; Aoki et al., 2007)	33.52 (Zhao et al., 2004)
	Predictions	25.25	29.45	34.62
	Relative deviation	2.32%	3.40%	3.28%
S/N/mm	Experiments	5.04 (Kuth and Pellegrino, 2007; Zhao, 2010)		
	Predictions	6.07		
	Relative deviation	20.44%		

woven fabric yarns is needed to predict tensile and in-plane shear strengths of the TWF composites.

It is worth pointing out that the failure criterion employed implies that the approach is capable of picking up the first sign of failure and there would be plenty of safety margin after the predicted shear failure. In order to obtain more accurate calculated results, the further works necessitates to consider the effects of nonlinear response and to conduct further experiments to determine the nonlinear properties of TWF composites. If more information about the above effects and influences are understood and implemented for assessment model of shear failure response, then more exact shear failure strength can be determined.

6. Conclusions

The focus of this paper has been to present novel micromechanical curved beam models for the prediction of tensile and in-plane shear strength of TWF composites by accounting for the interaction between angularly interlacing yarns. New analytical solutions of the models are derived to calculate tensile and in-plane shear strengths of TWF composites by means of the minimum total complementary potential energy principle founded on micromechanics. The applicability of the models for predicting tensile and in-plane shear strengths from fabric specifications and mechanical properties of constituents has been proved successfully. Reasonable correlation is achieved between the predictions and actual experimental results in prior literatures. The new analytical models presented in this paper are argued to be a valid and rational basis for tensile and in-plane shear strengths analysis of TWF composites.

Acknowledgment

This project was supported by NSFC (No. 51375033 and 51405006)

Appendix A. Definitions for transformation variables B_i

$$B_1 = \frac{h^2}{2EI_y}\int_0^{\frac{L}{2}}\left(\sin\frac{\pi x}{L}\right)^2\sqrt{1+\left(\frac{\pi h}{2L}\cos\frac{\pi x}{L}\right)^2}\,dx \tag{A-1}$$

$$B_2 = \frac{1}{2EI_y}\int_0^{\frac{L}{2}} x^2\sqrt{1+\left(\frac{\pi h}{2L}\cos\frac{\pi x}{L}\right)^2}\,dx \tag{A-2}$$

$$B_3 = \frac{-h}{EI_y}\int_0^{\frac{L}{2}} x\sin\frac{\pi x}{L}\sqrt{1+\left(\frac{\pi h}{2L}\cos\frac{\pi x}{L}\right)^2}\,dx \tag{A-3}$$

$$B_4 = \frac{2}{EA}\int_0^{\frac{L}{2}}\left[\sqrt{1+\left(\frac{\pi h}{2L}\cos\frac{\pi x}{L}\right)^2}\right]^{-1}dx \tag{A-4}$$

$$B_5 = \frac{h^2}{EI_y}\int_0^{L}\left(1-\cos\frac{\pi x}{L}\right)^2\sqrt{1+\left(\frac{\pi h}{2L}\sin\frac{\pi x}{L}\right)^2}\,dx \tag{A-5}$$

$$B_6 = \frac{1}{4EI_y}\int_0^{L} x^2\sqrt{1+\left(\frac{\pi h}{2L}\sin\frac{\pi x}{L}\right)^2}\,dx \tag{A-6}$$

$$B_7 = \frac{1}{EI_y}\int_0^{L}\sqrt{1+\left(\frac{\pi h}{2L}\sin\frac{\pi x}{L}\right)^2}\,dx \tag{A-7}$$

$$B_8 = -\frac{h}{EI_y}\int_0^{L} x\left(1-\cos\frac{\pi x}{L}\right)\sqrt{1+\left(\frac{\pi h}{2L}\sin\frac{\pi x}{L}\right)^2}\,dx \tag{A-8}$$

$$B_9 = -\frac{2h}{EI_y}\int_0^{L}\left(1-\cos\frac{\pi x}{L}\right)\sqrt{1+\left(\frac{\pi h}{2L}\sin\frac{\pi x}{L}\right)^2}\,dx \tag{A-9}$$

$$B_{10} = \frac{1}{EI_y}\int_0^{L} x\sqrt{1+\left(\frac{\pi h}{2L}\sin\frac{\pi x}{L}\right)^2}\,dx \tag{A-10}$$

$$B_{11} = \frac{4}{EA}\int_0^{L}\left[\sqrt{1+\left(\frac{\pi h}{2L}\sin\frac{\pi x_3}{L}\right)^2}\right]^{-1}dx_3 \tag{A-11}$$

Appendix B. Definitions for transformation variables C_i

$$C_1 = \frac{\begin{vmatrix} 4(B_5+B_{11}) & (2B_3-4B_8) & -4B_9 \\ -2B_8 & 4(B_2+2B_6) & 4B_{10} \\ -2B_9 & 4B_{10} & 8B_7 \end{vmatrix}}{\begin{vmatrix} 4(B_1+B_4)+8(B_5+B_{11}) & (2B_3-4B_8) & -4B_9 \\ (2B_3-4B_8) & 4(B_2+2B_6) & 4B_{10} \\ -4B_9 & 4B_{10} & 8B_7 \end{vmatrix}} \tag{B-1}$$

$$C_2 = \frac{\begin{vmatrix} 4(B_1+B_4)+8(B_5+B_{11}) & 4(B_5+B_{11}) & -4B_9 \\ (2B_3-4B_8) & -2B_8 & 4B_{10} \\ -4B_9 & -2B_9 & 8B_7 \end{vmatrix}}{\begin{vmatrix} 4(B_1+B_4)+8(B_5+B_{11}) & (2B_3-4B_8) & -4B_9 \\ (2B_3-4B_8) & 4(B_2+2B_6) & 4B_{10} \\ -4B_9 & 4B_{10} & 8B_7 \end{vmatrix}} \tag{B-2}$$

$$C_3 = \frac{\begin{vmatrix} 4(B_1+B_4)+8(B_5+B_{11}) & (2B_3-4B_8) & 4(B_5+B_{11}) \\ (2B_3-4B_8) & 4(B_2+2B_6) & -2B_8 \\ -4B_9 & 4B_{10} & -2B_9 \end{vmatrix}}{\begin{vmatrix} 4(B_1+B_4)+8(B_5+B_{11}) & (2B_3-4B_8) & -4B_9 \\ (2B_3-4B_8) & 4(B_2+2B_6) & 4B_{10} \\ -4B_9 & 4B_{10} & 8B_7 \end{vmatrix}} \tag{B-3}$$

Appendix C. Definitions for transformation variables Q_i

$$Q_1 = 2(K_{11}+K_{17}+K_{27}+K_{37}) \tag{C-1}$$

$$Q_2 = 2(K_{10}+K_{16}) \tag{C-2}$$

$$Q_3 = 2(K_{26}+K_{36}) \tag{C-3}$$

$$Q_4 = 2(K_1+K_4+K_{28}+K_{38}) \tag{C-4}$$

$$Q_5 = 2(K_6+K_{19}+K_{40}) \tag{C-5}$$

$$Q_6 = 2(K_3+K_5+K_{12}+K_{18}+K_{29}+K_{39}) \tag{C-6}$$

$$Q_7 = 2(K_{13}+K_{20}) \tag{C-7}$$

$$Q_8 = 2(K_{30}+K_{41}) \tag{C-8}$$

$$Q_9 = 2(K_{33}+K_{45}) \tag{C-9}$$

$$Q_{10} = 2(K_{24}+K_{47}) \tag{C-10}$$

$$Q_{11} = 2(K_{15}+K_{23}+K_{34}+K_{46}) \tag{C-11}$$

$$Q_{12} = 2K_{22} \tag{C-12}$$

$$Q_{13} = 2(K_{14}+K_{21}) \tag{C-13}$$

$$Q_{14} = 2(K_{31}+K_{42}) \tag{C-14}$$

$$Q_{15} = 2K_{44} \tag{C-15}$$

$$Q_{16} = 2(K_{32}+K_{43}) \tag{C-16}$$

$$Q_{17} = 2(K_8+K_{49}) \tag{C-17}$$

$$Q_{18} = 2(K_2+K_7+K_{35}+K_{48}) \tag{C-18}$$

$$Q_{19} = 2(K_9+K_{25}+K_{50}) \tag{C-19}$$

$$Q_{20} = J_9+J_{12}+J_{18}+J_{28}+J_{31}+J_{37}+J_{47} \tag{C-20}$$

$$Q_{21} = J_8+J_{11}+J_{17} \tag{C-21}$$

$$Q_{22} = J_{27}+J_{30}+J_{36}+J_{46} \tag{C-22}$$

$$Q_{23} = J_1+J_2+J_{32}+J_{38}+J_{48} \tag{C-23}$$

$$Q_{24} = J_6+J_{20}+J_{50} \tag{C-24}$$

$$Q_{25} = J_3+J_5+J_{13}+J_{19}+J_{39}+J_{49} \tag{C-25}$$

$$Q_{26} = J_{10}+J_{14}+J_{21} \tag{C-26}$$

$$Q_{27} = J_{29}+J_{33}+J_{40}+J_{51} \tag{C-27}$$

$$Q_{28} = J_{35}+J_{43}+J_{55} \tag{C-28}$$

$$Q_{29} = J_{25}+J_{57} \tag{C-29}$$

$$Q_{30} = J_{16}+J_{24}+J_{44}+J_{56} \tag{C-30}$$

$$Q_{31} = J_{23} \tag{C-31}$$

$$Q_{32} = J_{15}+J_{22} \tag{C-32}$$

$$Q_{33} = J_{34}+J_{41}+J_{52} \tag{C-33}$$

$$Q_{34} = J_{54} \tag{C-34}$$

$$Q_{35} = J_{42}+J_{53} \tag{C-35}$$

$$Q_{36} = J_{59} \tag{C-36}$$

$$Q_{37} = J_4+J_{45}+J_{58} \tag{C-37}$$

$$Q_{38} = J_7+J_{26}+J_{60} \tag{C-38}$$

Appendix D. Definitions for transformation variables K_i

$$K_1 = \frac{1}{EI_y}\int_0^{\frac{L}{3}} x^2\sqrt{1+\left(\frac{\pi h}{2L}\cos\frac{\pi x}{L}\right)^2}\,dx \tag{D-1}$$

$$K_2 = -\frac{h}{EI_y}\int_0^{\frac{L}{3}} x\sin\frac{\pi x}{L}\sqrt{1+\left(\frac{\pi h}{2L}\cos\frac{\pi x}{L}\right)^2}\,dx \tag{D-2}$$

$$K_3 = \frac{h^2}{16EI_y}\int_0^{\frac{L}{3}} \left(\sin\frac{\pi x}{L}\right)^2\sqrt{1+\left(\frac{\pi h}{2L}\cos\frac{\pi x}{L}\right)^2}\,dx \tag{D-3}$$

$$K_4 = \frac{L^2}{9EI_y}\int_{\frac{L}{3}}^{\frac{L}{2}} \sqrt{1+\left(\frac{\pi h}{2L}\cos\frac{\pi x}{L}\right)^2}\,dx \tag{D-4}$$

$$K_5 = \frac{h^2}{16EI_y}\int_{\frac{L}{3}}^{\frac{L}{2}} \left(\sin\frac{\pi x}{L}\right)^2\sqrt{1+\left(\frac{\pi h}{2L}\cos\frac{\pi x}{L}\right)^2}\,dx \tag{D-5}$$

$$K_6 = \frac{3h^2}{64EI_y}\int_{\frac{L}{3}}^{\frac{L}{2}} \left(2\sin\frac{\pi x}{L} - \sqrt{3}\right)^2 \sqrt{1+\left(\frac{\pi h}{2L}\cos\frac{\pi x}{L}\right)^2}\,dx \tag{D-6}$$

$$K_7 = -\frac{hL}{6EI_y}\int_{\frac{L}{3}}^{\frac{L}{2}} \sin\frac{\pi x}{L}\sqrt{1+\left(\frac{\pi h}{2L}\cos\frac{\pi x}{L}\right)^2}\,dx \tag{D-7}$$

$$K_8 = \frac{hL\sqrt{3}}{12EI_y}\int_{\frac{L}{3}}^{\frac{L}{2}} \left(2\sin\frac{\pi x}{L} - \sqrt{3}\right)\sqrt{1+\left(\frac{\pi h}{2L}\cos\frac{\pi x}{L}\right)^2}\,dx \tag{D-8}$$

$$K_9 = -\frac{h^2\sqrt{3}}{16EI_y}\int_{\frac{L}{3}}^{\frac{L}{2}} \left(2\sin\frac{\pi x}{L} - \sqrt{3}\right) \times\left(\sin\frac{\pi x}{L}\right)\sqrt{1+\left(\frac{\pi h}{2L}\cos\frac{\pi x}{L}\right)^2}\,dx \tag{D-9}$$

$$K_{10} = \frac{1}{EI_z}\int_0^{\frac{L}{3}} \sqrt{1+\left(\frac{\pi h}{2L}\cos\frac{\pi x}{L}\right)^2}\,dx \tag{D-10}$$

$$K_{11} = \frac{1}{EI_z}\int_0^{\frac{L}{3}} x^2\sqrt{1+\left(\frac{\pi h}{2L}\cos\frac{\pi x}{L}\right)^2}\,dx \tag{D-11}$$

$$K_{12} = \frac{3}{4EI_z}\int_0^{\frac{L}{3}} x^2\sqrt{1+\left(\frac{\pi h}{2L}\cos\frac{\pi x}{L}\right)^2}\,dx \tag{D-12}$$

$$K_{13} = -\frac{2}{EI_z}\int_0^{\frac{L}{3}} x\sqrt{1+\left(\frac{\pi h}{2L}\cos\frac{\pi x}{L}\right)^2}\,dx \tag{D-13}$$

$$K_{14} = \frac{\sqrt{3}}{EI_z}\int_0^{\frac{L}{3}} x\sqrt{1+\left(\frac{\pi h}{2L}\cos\frac{\pi x}{L}\right)^2}\,dx \tag{D-14}$$

$$K_{15} = -\frac{\sqrt{3}}{EI_z}\int_0^{\frac{L}{3}} x^2\sqrt{1+\left(\frac{\pi h}{2L}\cos\frac{\pi x}{L}\right)^2}\,dx \tag{D-15}$$

$$K_{16} = \frac{1}{EI_z}\int_{\frac{L}{3}}^{\frac{L}{2}} \sqrt{1+\left(\frac{\pi h}{2L}\cos\frac{\pi x}{L}\right)^2}\,dx \tag{D-16}$$

$$K_{17} = \frac{1}{EI_z}\int_{\frac{L}{3}}^{\frac{L}{2}} x^2\sqrt{1+\left(\frac{\pi h}{2L}\cos\frac{\pi x}{L}\right)^2}\,dx \tag{D-17}$$

$$K_{18} = \frac{1}{16EI_z}\int_{\frac{L}{3}}^{\frac{L}{2}} \left(2x\sqrt{3}+b\right)^2\sqrt{1+\left(\frac{\pi h}{2L}\cos\frac{\pi x}{L}\right)^2}\,dx \tag{D-18}$$

$$K_{19} = \frac{1}{16EI_z}\int_{\frac{L}{3}}^{\frac{L}{2}} \left(2x+b\sqrt{3}\right)^2\sqrt{1+\left(\frac{\pi h}{2L}\cos\frac{\pi x}{L}\right)^2}\,dx \tag{D-19}$$

$$K_{20} = -\frac{2}{EI_z}\int_{\frac{L}{3}}^{\frac{L}{2}} x\sqrt{1+\left(\frac{\pi h}{2L}\cos\frac{\pi x}{L}\right)^2}\,dx \tag{D-20}$$

$$K_{21} = \frac{1}{2EI_z}\int_{\frac{L}{3}}^{\frac{L}{2}} \left(2x\sqrt{3}+b\right)\sqrt{1+\left(\frac{\pi h}{2L}\cos\frac{\pi x}{L}\right)^2}\,dx \tag{D-21}$$

$$K_{22} = \frac{1}{2EI_z}\int_{\frac{L}{3}}^{\frac{L}{2}} \left(2x+b\sqrt{3}\right)\sqrt{1+\left(\frac{\pi h}{2L}\cos\frac{\pi x}{L}\right)^2}\,dx \tag{D-22}$$

$$K_{23} = -\frac{1}{2EI_z}\int_{\frac{L}{3}}^{\frac{L}{2}} x\left(2x\sqrt{3}+b\right)\sqrt{1+\left(\frac{\pi h}{2L}\cos\frac{\pi x}{L}\right)^2}\,dx \tag{D-23}$$

$$K_{24} = -\frac{1}{2EI_z}\int_{\frac{L}{3}}^{\frac{L}{2}} x\left(2x+b\sqrt{3}\right)\sqrt{1+\left(\frac{\pi h}{2L}\cos\frac{\pi x}{L}\right)^2}\,dx \tag{D-24}$$

$$K_{25} = \frac{1}{8EI_z}\int_{\frac{L}{3}}^{\frac{L}{2}} \left(2x\sqrt{3}+b\right)\left(2x+b\sqrt{3}\right)\sqrt{1+\left(\frac{\pi h}{2L}\cos\frac{\pi x}{L}\right)^2}\,dx \tag{D-25}$$

$$K_{26} = \frac{1}{GI_p}\int_0^{\frac{L}{3}} \sqrt{1+\left(\frac{\pi h}{2L}\cos\frac{\pi x}{L}\right)^2}\,dx \tag{D-26}$$

$$K_{27} = \frac{h^2}{4GI_p}\int_0^{\frac{L}{3}} \left(\sin\frac{\pi x}{L}\right)^2\sqrt{1+\left(\frac{\pi h}{2L}\cos\frac{\pi x}{L}\right)^2}\,dx \tag{D-27}$$

$$K_{28} = \frac{b^2}{4GI_p}\int_0^{\frac{L}{3}} \sqrt{1+\left(\frac{\pi h}{2L}\cos\frac{\pi x}{L}\right)^2}\,dx \tag{D-28}$$

$$K_{29} = \frac{3h^2}{16GI_p}\int_0^{\frac{L}{3}} \left(\sin\frac{\pi x}{L}\right)^2\sqrt{1+\left(\frac{\pi h}{2L}\cos\frac{\pi x}{L}\right)^2}\,dx \tag{D-29}$$

$$K_{30} = \frac{h}{GI_p}\int_0^{\frac{L}{3}} \left(\sin\frac{\pi x}{L}\right)\sqrt{1+\left(\frac{\pi h}{2L}\cos\frac{\pi x}{L}\right)^2}\,dx \tag{D-30}$$

$$K_{31} = -\frac{b}{GI_p}\int_0^{\frac{L}{3}} \sqrt{1+\left(\frac{\pi h}{2L}\cos\frac{\pi x}{L}\right)^2}\,dx \tag{D-31}$$

$$K_{32} = -\frac{h\sqrt{3}}{2GI_p}\int_0^{\frac{L}{3}} \left(\sin\frac{\pi x}{L}\right)\sqrt{1+\left(\frac{\pi h}{2L}\cos\frac{\pi x}{L}\right)^2}\,dx \tag{D-32}$$

$$K_{33} = -\frac{bh}{2GI_p}\int_0^{\frac{L}{3}} \left(\sin\frac{\pi x}{L}\right)\sqrt{1+\left(\frac{\pi h}{2L}\cos\frac{\pi x}{L}\right)^2}\,dx \tag{D-33}$$

$$K_{34} = -\frac{h^2\sqrt{3}}{4GI_p}\int_0^{\frac{L}{3}} \left(\sin\frac{\pi x}{L}\right)^2\sqrt{1+\left(\frac{\pi h}{2L}\cos\frac{\pi x}{L}\right)^2}\,dx \tag{D-34}$$

$$K_{35} = \frac{bh\sqrt{3}}{4GI_p}\int_0^{\frac{L}{3}} \left(\sin\frac{\pi x}{L}\right)\sqrt{1+\left(\frac{\pi h}{2L}\cos\frac{\pi x}{L}\right)^2}\,dx \tag{D-35}$$

$$K_{36} = \frac{1}{GI_p}\int_{\frac{L}{3}}^{\frac{L}{2}} \sqrt{1+\left(\frac{\pi h}{2L}\cos\frac{\pi x}{L}\right)^2}\,dx \tag{D-36}$$

$$K_{37} = \frac{h^2}{4GI_p}\int_{\frac{L}{3}}^{\frac{L}{2}} \left(\sin\frac{\pi x}{L}\right)^2\sqrt{1+\left(\frac{\pi h}{2L}\cos\frac{\pi x}{L}\right)^2}\,dx \tag{D-37}$$

$$K_{38} = \frac{b^2}{GI_p}\int_{\frac{L}{3}}^{\frac{L}{2}} \sqrt{1+\left(\frac{\pi h}{2L}\cos\frac{\pi x}{L}\right)^2}\,dx \tag{D-38}$$

$$K_{39}=\frac{3h^2}{16GI_p}\int_{\frac{L}{3}}^{\frac{L}{2}}\left(\sin\frac{\pi x}{L}\right)^2\sqrt{1+\left(\frac{\pi h}{2L}\cos\frac{\pi x}{L}\right)^2}dx \tag{D-39}$$

$$K_{40}=\frac{h^2}{64GI_p}\int_{\frac{L}{3}}^{\frac{L}{2}}\left(2\sin\frac{\pi x}{L}-\sqrt{3}\right)^2\sqrt{1+\left(\frac{\pi h}{2L}\cos\frac{\pi x}{L}\right)^2}dx \tag{D-40}$$

$$K_{41}=\frac{h}{GI_p}\int_{\frac{L}{3}}^{\frac{L}{2}}\left(\sin\frac{\pi x}{L}\right)\sqrt{1+\left(\frac{\pi h}{2L}\cos\frac{\pi x}{L}\right)^2}dx \tag{D-41}$$

$$K_{42}=-\frac{2b}{GI_p}\int_{\frac{L}{3}}^{\frac{L}{2}}\sqrt{1+\left(\frac{\pi h}{2L}\cos\frac{\pi x}{L}\right)^2}dx \tag{D-42}$$

$$K_{43}=-\frac{h\sqrt{3}}{2GI_p}\int_{\frac{L}{3}}^{\frac{L}{2}}\left(\sin\frac{\pi x}{L}\right)\sqrt{1+\left(\frac{\pi h}{2L}\cos\frac{\pi x}{L}\right)^2}dx \tag{D-43}$$

$$K_{44}=-\frac{h}{4GI_p}\int_{\frac{L}{3}}^{\frac{L}{2}}\left(2\sin\frac{\pi x}{L}-\sqrt{3}\right)\sqrt{1+\left(\frac{\pi h}{2L}\cos\frac{\pi x}{L}\right)^2}dx \tag{D-44}$$

$$K_{45}=-\frac{bh}{GI_p}\int_{\frac{L}{3}}^{\frac{L}{2}}\left(\sin\frac{\pi x}{L}\right)\sqrt{1+\left(\frac{\pi h}{2L}\cos\frac{\pi x}{L}\right)^2}dx \tag{D-45}$$

$$K_{46}=-\frac{h^2\sqrt{3}}{4GI_p}\int_{\frac{L}{3}}^{\frac{L}{2}}\left(\sin\frac{\pi x}{L}\right)^2\sqrt{1+\left(\frac{\pi h}{2L}\cos\frac{\pi x}{L}\right)^2}dx \tag{D-46}$$

$$K_{47}=-\frac{h^2}{8GI_p}\int_{\frac{L}{3}}^{\frac{L}{2}}\left(\sin\frac{\pi x}{L}\right)\left(2\sin\frac{\pi x}{L}-\sqrt{3}\right)\times\sqrt{1+\left(\frac{\pi h}{2L}\cos\frac{\pi x}{L}\right)^2}dx \tag{D-47}$$

$$K_{48}=\frac{bh\sqrt{3}}{2GI_p}\int_{\frac{L}{3}}^{\frac{L}{2}}\left(\sin\frac{\pi x}{L}\right)\sqrt{1+\left(\frac{\pi h}{2L}\cos\frac{\pi x}{L}\right)^2}dx \tag{D-48}$$

$$K_{49}=\frac{bh}{4GI_p}\int_{\frac{L}{3}}^{\frac{L}{2}}\left(2\sin\frac{\pi x}{L}-\sqrt{3}\right)\sqrt{1+\left(\frac{\pi h}{2L}\cos\frac{\pi x}{L}\right)^2}dx \tag{D-49}$$

$$K_{50}=\frac{h^2\sqrt{3}}{16GI_p}\int_{\frac{L}{3}}^{\frac{L}{2}}\left(2\sin\frac{\pi x}{L}-\sqrt{3}\right)\left(\sin\frac{\pi x}{L}\right)\times\sqrt{1+\left(\frac{\pi h}{2L}\cos\frac{\pi x}{L}\right)^2}dx \tag{D-50}$$

Appendix E. Definitions for transformation variables J_i

$$J_1=\frac{1}{36EI_y}\int_{\frac{L}{6}}^{\frac{L}{2}}(6x-L)^2\sqrt{1+\left(\frac{\pi h}{2L}\sin\frac{\pi x}{L}\right)^2}dx \tag{E-1}$$

$$J_2=\frac{1}{36EI_y}\int_{\frac{L}{2}}^{\frac{5L}{6}}(6x-5L)^2\sqrt{1+\left(\frac{\pi h}{2L}\sin\frac{\pi x}{L}\right)^2}dx \tag{E-2}$$

$$J_3=\frac{h^2}{16EI_y}\int_{\frac{L}{2}}^{\frac{5L}{6}}\left(\cos\frac{\pi x}{L}\right)^2\sqrt{1+\left(\frac{\pi h}{2L}\sin\frac{\pi x}{L}\right)^2}dx \tag{E-3}$$

$$J_4=\frac{h}{12EI_y}\int_{\frac{L}{2}}^{\frac{5L}{6}}\left(\cos\frac{\pi x}{L}\right)(6x-5L)\sqrt{1+\left(\frac{\pi h}{2L}\sin\frac{\pi x}{L}\right)^2}dx \tag{E-4}$$

$$J_5=\frac{h^2}{16EI_y}\int_{\frac{5L}{6}}^{L}\left(\cos\frac{\pi x}{L}\right)^2\sqrt{1+\left(\frac{\pi h}{2L}\sin\frac{\pi x}{L}\right)^2}dx \tag{E-5}$$

$$J_6=\frac{3h^2}{64EI_y}\int_{\frac{5L}{6}}^{L}\left(\sqrt{3}-2\cos\frac{\pi x}{L}\right)^2\sqrt{1+\left(\frac{\pi h}{2L}\sin\frac{\pi x}{L}\right)^2}dx \tag{E-6}$$

$$J_7=\frac{h^2\sqrt{3}}{16EI_y}\int_{\frac{5L}{6}}^{L}\left(\sqrt{3}-2\cos\frac{\pi x}{L}\right)\left(\cos\frac{\pi x}{L}\right)\sqrt{1+\left(\frac{\pi h}{2L}\sin\frac{\pi x}{L}\right)^2}dx \tag{E-7}$$

$$J_8=\frac{1}{EI_z}\int_0^{\frac{L}{2}}\sqrt{1+\left(\frac{\pi h}{2L}\sin\frac{\pi x}{L}\right)^2}dx \tag{E-8}$$

$$J_9=\frac{1}{EI_z}\int_0^{\frac{L}{2}}x^2\sqrt{1+\left(\frac{\pi h}{2L}\sin\frac{\pi x}{L}\right)^2}dx \tag{E-9}$$

$$J_{10}=-\frac{2}{EI_z}\int_0^{\frac{L}{2}}x\sqrt{1+\left(\frac{\pi h}{2L}\sin\frac{\pi x}{L}\right)^2}dx \tag{E-10}$$

$$J_{11}=\frac{1}{EI_z}\int_{\frac{L}{2}}^{\frac{5L}{6}}\sqrt{1+\left(\frac{\pi h}{2L}\sin\frac{\pi x}{L}\right)^2}dx \tag{E-11}$$

$$J_{12}=\frac{1}{EI_z}\int_{\frac{L}{2}}^{\frac{5L}{6}}x^2\sqrt{1+\left(\frac{\pi h}{2L}\sin\frac{\pi x}{L}\right)^2}dx \tag{E-12}$$

$$J_{13}=\frac{1}{16EI_z}\int_{\frac{L}{2}}^{\frac{5L}{6}}\left(2x\sqrt{3}+b-L\sqrt{3}\right)^2\sqrt{1+\left(\frac{\pi h}{2L}\sin\frac{\pi x}{L}\right)^2}dx \tag{E-13}$$

$$J_{14}=-\frac{2}{EI_z}\int_{\frac{L}{2}}^{\frac{5L}{6}}x\sqrt{1+\left(\frac{\pi h}{2L}\sin\frac{\pi x}{L}\right)^2}dx \tag{E-14}$$

$$J_{15}=\frac{1}{2EI_z}\int_{\frac{L}{2}}^{\frac{5L}{6}}\left(2x\sqrt{3}+b-L\sqrt{3}\right)\sqrt{1+\left(\frac{\pi h}{2L}\sin\frac{\pi x}{L}\right)^2}\,dx \tag{E-15}$$

$$J_{16}=-\frac{1}{2EI_z}\int_{\frac{L}{2}}^{\frac{5L}{6}}x\left(2x\sqrt{3}+b-L\sqrt{3}\right)\sqrt{1+\left(\frac{\pi h}{2L}\sin\frac{\pi x}{L}\right)^2}\,dx \tag{E-16}$$

$$J_{17}=\frac{1}{EI_z}\int_{\frac{5L}{6}}^{L}\sqrt{1+\left(\frac{\pi h}{2L}\sin\frac{\pi x}{L}\right)^2}\,dx \tag{E-17}$$

$$J_{18}=\frac{1}{EI_z}\int_{\frac{5L}{6}}^{L}x^2\sqrt{1+\left(\frac{\pi h}{2L}\sin\frac{\pi x}{L}\right)^2}\,dx \tag{E-18}$$

$$J_{19}=\frac{1}{16EI_z}\int_{\frac{5L}{6}}^{L}\left(2x\sqrt{3}+b-L\sqrt{3}\right)^2\sqrt{1+\left(\frac{\pi h}{2L}\sin\frac{\pi x}{L}\right)^2}\,dx \tag{E-19}$$

$$J_{20}=\frac{1}{144EI_z}\int_{\frac{5L}{6}}^{L}\left(6x+3b\sqrt{3}-5L\right)^2\sqrt{1+\left(\frac{\pi h}{2L}\sin\frac{\pi x}{L}\right)^2}\,dx \tag{E-20}$$

$$J_{21}=-\frac{2}{EI_z}\int_{\frac{5L}{6}}^{L}x\sqrt{1+\left(\frac{\pi h}{2L}\sin\frac{\pi x}{L}\right)^2}\,dx \tag{E-21}$$

$$J_{22}=\frac{1}{2EI_z}\int_{\frac{5L}{6}}^{L}\left(2x\sqrt{3}+b-L\sqrt{3}\right)\sqrt{1+\left(\frac{\pi h}{2L}\sin\frac{\pi x}{L}\right)^2}\,dx \tag{E-22}$$

$$J_{23}=\frac{1}{6EI_z}\int_{\frac{5L}{6}}^{L}\left(6x+3b\sqrt{3}-5L\right)\sqrt{1+\left(\frac{\pi h}{2L}\sin\frac{\pi x}{L}\right)^2}\,dx \tag{E-23}$$

$$J_{24}=-\frac{1}{2EI_z}\int_{\frac{5L}{6}}^{L}x\left(2x\sqrt{3}+b-L\sqrt{3}\right)\sqrt{1+\left(\frac{\pi h}{2L}\sin\frac{\pi x}{L}\right)^2}\,dx \tag{E-24}$$

$$J_{25}=-\frac{1}{6EI_z}\int_{\frac{5L}{6}}^{L}x\left(6x+3b\sqrt{3}-5L\right)\sqrt{1+\left(\frac{\pi h}{2L}\sin\frac{\pi x}{L}\right)^2}\,dx \tag{E-25}$$

$$J_{26}=\frac{1}{24EI_z}\int_{\frac{5L}{6}}^{L}\left(24x\sqrt{3}+12b-12L\sqrt{3}\right)\left(6x+3b\sqrt{3}-5L\right)\times\sqrt{1+\left(\frac{\pi h}{2L}\sin\frac{\pi x}{L}\right)^2}\,dx \tag{E-26}$$

$$J_{27}=\frac{1}{GI_p}\int_{0}^{\frac{L}{6}}\sqrt{1+\left(\frac{\pi h}{2L}\sin\frac{\pi x}{L}\right)^2}\,dx \tag{E-27}$$

$$J_{28}=\frac{h^2}{4GI_p}\int_{0}^{\frac{L}{6}}\left(1-\cos\frac{\pi x}{L}\right)^2\sqrt{1+\left(\frac{\pi h}{2L}\sin\frac{\pi x}{L}\right)^2}\,dx \tag{E-28}$$

$$J_{29}=\frac{h}{GI_p}\int_{0}^{\frac{L}{6}}\left(1-\cos\frac{\pi x}{L}\right)\sqrt{1+\left(\frac{\pi h}{2L}\sin\frac{\pi x}{L}\right)^2}\,dx \tag{E-29}$$

$$J_{30}=\frac{1}{GI_p}\int_{\frac{L}{6}}^{\frac{L}{2}}\sqrt{1+\left(\frac{\pi h}{2L}\sin\frac{\pi x}{L}\right)^2}\,dx \tag{E-30}$$

$$J_{31}=\frac{h^2}{4GI_p}\int_{\frac{L}{6}}^{\frac{L}{2}}\left(1-\cos\frac{\pi x}{L}\right)^2\sqrt{1+\left(\frac{\pi h}{2L}\sin\frac{\pi x}{L}\right)^2}\,dx \tag{E-31}$$

$$J_{32}=\frac{b^2}{4GI_p}\int_{\frac{L}{6}}^{\frac{L}{2}}\sqrt{1+\left(\frac{\pi h}{2L}\sin\frac{\pi x}{L}\right)^2}\,dx \tag{E-32}$$

$$J_{33}=\frac{h}{GI_p}\int_{\frac{L}{6}}^{\frac{L}{2}}\left(1-\cos\frac{\pi x}{L}\right)\sqrt{1+\left(\frac{\pi h}{2L}\sin\frac{\pi x}{L}\right)^2}\,dx \tag{E-33}$$

$$J_{34}=-\frac{b}{GI_p}\int_{\frac{L}{6}}^{\frac{L}{2}}\sqrt{1+\left(\frac{\pi h}{2L}\sin\frac{\pi x}{L}\right)^2}\,dx \tag{E-34}$$

$$J_{35}=-\frac{bh}{2GI_p}\int_{\frac{L}{6}}^{\frac{L}{2}}\left(1-\cos\frac{\pi x}{L}\right)\sqrt{1+\left(\frac{\pi h}{2L}\sin\frac{\pi x}{L}\right)^2}\,dx \tag{E-35}$$

$$J_{36}=\frac{1}{GI_p}\int_{\frac{L}{2}}^{\frac{5L}{6}}\sqrt{1+\left(\frac{\pi h}{2L}\sin\frac{\pi x}{L}\right)^2}\,dx \tag{E-36}$$

$$J_{37}=\frac{h^2}{4GI_p}\int_{\frac{L}{2}}^{\frac{5L}{6}}\left(1-\cos\frac{\pi x}{L}\right)^2\sqrt{1+\left(\frac{\pi h}{2L}\sin\frac{\pi x}{L}\right)^2}\,dx \tag{E-37}$$

$$J_{38}=\frac{9b^2}{4GI_p}\int_{\frac{L}{2}}^{\frac{5L}{6}}\sqrt{1+\left(\frac{\pi h}{2L}\sin\frac{\pi x}{L}\right)^2}\,dx \tag{E-38}$$

$$J_{39}=\frac{3h^2}{16GI_p}\int_{\frac{L}{2}}^{\frac{5L}{6}}\left(\cos\frac{\pi x}{L}\right)^2\sqrt{1+\left(\frac{\pi h}{2L}\sin\frac{\pi x}{L}\right)^2}\,dx \tag{E-39}$$

$$J_{40}=\frac{h}{GI_p}\int_{\frac{L}{2}}^{\frac{5L}{6}}\left(1-\cos\frac{\pi x}{L}\right)\sqrt{1+\left(\frac{\pi h}{2L}\sin\frac{\pi x}{L}\right)^2}\,dx \tag{E-40}$$

$$J_{41}=-\frac{3b}{GI_p}\int_{\frac{L}{2}}^{\frac{5L}{6}}\sqrt{1+\left(\frac{\pi h}{2L}\sin\frac{\pi x}{L}\right)^2}\,dx \tag{E-41}$$

$$J_{42}=\frac{h\sqrt{3}}{2GI_p}\int_{\frac{L}{2}}^{\frac{5L}{6}}\left(\cos\frac{\pi x}{L}\right)\sqrt{1+\left(\frac{\pi h}{2L}\sin\frac{\pi x}{L}\right)^2}\,dx \tag{E-42}$$

$$J_{43}=-\frac{3bh}{2GI_p}\int_{\frac{L}{2}}^{\frac{5L}{6}}\left(1-\cos\frac{\pi x}{L}\right)\sqrt{1+\left(\frac{\pi h}{2L}\sin\frac{\pi x}{L}\right)^2}\,dx \tag{E-43}$$

$$J_{44}=\frac{h^2\sqrt{3}}{4GI_p}\int_{\frac{L}{2}}^{\frac{5L}{6}}\left(1-\cos\frac{\pi x}{L}\right)\left(\cos\frac{\pi x}{L}\right)\sqrt{1+\left(\frac{\pi h}{2L}\sin\frac{\pi x}{L}\right)^2}\,dx \tag{E-44}$$

$$J_{45} = -\frac{3bh\sqrt{3}}{4GI_p}\int_{\frac{L}{2}}^{\frac{5L}{6}}\left(\cos\frac{\pi x}{L}\right)\sqrt{1+\left(\frac{\pi h}{2L}\sin\frac{\pi x}{L}\right)^2}\,dx \quad \text{(E-45)}$$

$$J_{46} = \frac{1}{GI_p}\int_{\frac{5L}{6}}^{L}\sqrt{1+\left(\frac{\pi h}{2L}\sin\frac{\pi x}{L}\right)^2}\,dx \quad \text{(E-46)}$$

$$J_{47} = \frac{h^2}{4GI_p}\int_{\frac{5L}{6}}^{L}\left(1-\cos\frac{\pi x}{L}\right)^2\sqrt{1+\left(\frac{\pi h}{2L}\sin\frac{\pi x}{L}\right)^2}\,dx \quad \text{(E-47)}$$

$$J_{48} = \frac{4b^2}{GI_p}\int_{\frac{5L}{6}}^{L}\sqrt{1+\left(\frac{\pi h}{2L}\sin\frac{\pi x}{L}\right)^2}\,dx \quad \text{(E-48)}$$

$$J_{49} = \frac{3h^2}{16GI_p}\int_{\frac{5L}{6}}^{L}\left(\cos\frac{\pi x}{L}\right)^2\sqrt{1+\left(\frac{\pi h}{2L}\sin\frac{\pi x}{L}\right)^2}\,dx \quad \text{(E-49)}$$

$$J_{50} = \frac{h^2}{64GI_p}\int_{\frac{5L}{6}}^{L}\left(\sqrt{3}-2\cos\frac{\pi x}{L}\right)^2\sqrt{1+\left(\frac{\pi h}{2L}\sin\frac{\pi x}{L}\right)^2}\,dx \quad \text{(E-50)}$$

$$J_{51} = \frac{h}{GI_p}\int_{\frac{5L}{6}}^{L}\left(1-\cos\frac{\pi x}{L}\right)\sqrt{1+\left(\frac{\pi h}{2L}\sin\frac{\pi x}{L}\right)^2}\,dx \quad \text{(E-51)}$$

$$J_{52} = -\frac{4b}{GI_p}\int_{\frac{5L}{6}}^{L}\sqrt{1+\left(\frac{\pi h}{2L}\sin\frac{\pi x}{L}\right)^2}\,dx \quad \text{(E-52)}$$

$$J_{53} = \frac{h\sqrt{3}}{2GI_p}\int_{\frac{5L}{6}}^{L}\left(\cos\frac{\pi x}{L}\right)\sqrt{1+\left(\frac{\pi h}{2L}\sin\frac{\pi x}{L}\right)^2}\,dx \quad \text{(E-53)}$$

$$J_{54} = -\frac{h}{4GI_p}\int_{\frac{5L}{6}}^{L}\left(\sqrt{3}-2\cos\frac{\pi x}{L}\right)\sqrt{1+\left(\frac{\pi h}{2L}\sin\frac{\pi x}{L}\right)^2}\,dx \quad \text{(E-54)}$$

$$J_{55} = -\frac{2bh}{GI_p}\int_{\frac{5L}{6}}^{L}\left(1-\cos\frac{\pi x}{L}\right)\sqrt{1+\left(\frac{\pi h}{2L}\sin\frac{\pi x}{L}\right)^2}\,dx \quad \text{(E-55)}$$

$$J_{56} = \frac{h^2\sqrt{3}}{4GI_p}\int_{\frac{5L}{6}}^{L}\left(1-\cos\frac{\pi x}{L}\right)\left(\cos\frac{\pi x}{L}\right)\sqrt{1+\left(\frac{\pi h}{2L}\sin\frac{\pi x}{L}\right)^2}\,dx \quad \text{(E-56)}$$

$$J_{57} = -\frac{h^2}{8GI_p}\int_{\frac{5L}{6}}^{L}\left(1-\cos\frac{\pi x}{L}\right)\left(\sqrt{3}-2\cos\frac{\pi x}{L}\right)\times\sqrt{1+\left(\frac{\pi h}{2L}\sin\frac{\pi x}{L}\right)^2}\,dx \quad \text{(E-57)}$$

$$J_{58} = -\frac{bh\sqrt{3}}{GI_p}\int_{\frac{5L}{6}}^{L}\left(\cos\frac{\pi x}{L}\right)\sqrt{1+\left(\frac{\pi h}{2L}\sin\frac{\pi x}{L}\right)^2}\,dx \quad \text{(E-58)}$$

$$J_{59} = \frac{bh}{2GI_p}\int_{\frac{5L}{6}}^{L}\left(\sqrt{3}-2\cos\frac{\pi x}{L}\right)\sqrt{1+\left(\frac{\pi h}{2L}\sin\frac{\pi x}{L}\right)^2}\,dx \quad \text{(E-59)}$$

$$J_{60} = -\frac{h^2\sqrt{3}}{16GI_p}\int_{\frac{5L}{6}}^{L}\left(\cos\frac{\pi x}{L}\right)\left(\sqrt{3}-2\cos\frac{\pi x}{L}\right)\times\sqrt{1+\left(\frac{\pi h}{2L}\sin\frac{\pi x}{L}\right)^2}\,dx \quad \text{(E-60)}$$

References

Callus, P.J., Mouritz, A.P., Bannister, M.K., Leong, K.H., 1999. Tensile properties and failure mechanisms of 3D woven GRP composites. Composites Part A 30 (11), 1277–1287.

Cheng, X., Xiong, J.J., 2009. A novel analytical model for predicting the compression modulus of 2D PWF composites. Compos. Struct. 88 (2), 296–303.

Xiong, J.J., Shenoi, R.A., Cheng, X., 2009. A modified micromechanical curved beam analytical model to predict the tension modulus of 2D plain weave fabric composites. Composites Part B 40 (8), 776–783.

Mahadik, Y., Hallett, S.R., 2011. Effect of fabric compaction and yarn waviness on 3D woven composite compressive properties. Composites Part A 42 (11), 1592–1600.

Cheng, X., Xiong, J.J., Bai, J.B., 2012. An analytical solution to predict the shear modulus of 2D plain weave fabric composites. Chin. J. Aeronaut. 25 (4), 575–583.

Bakar, I.A.A., Kramer, O., Bordas, S., Rabczuk, T., 2013. Optimization of elastic properties and weaving patterns of woven composites. Compos. Struct. 100, 575–591.

Aoki, T., Yoshida, K., 2006. Mechanical and thermal behaviors of triaxially-woven carbon/epoxy fabric composite. 47th AIAA/ASME/ASCE/AHS/ASC Structures, Structural Dynamics and Materials Conference, Rhode Island: Newport, May 1–4.

Aoki, T., Yoshida, K., Watanabe, A., 2007. Feasibility study of triaxially-woven fabric composite for deployable structures. 48th AIAA/ASME/ASCE/AHS/ASC Structures, Structural Dynamics and Materials Conference, Hawaii: Honolulu, April 23–26.

Kosugi, Y., Aoki, T., Watanabe, A., 2011. Fatigue characteristic and damage accumulation mechanism of triaxially-woven fabric composite. 52nd AIAA/ASME/ASCE/AHS/ASC Structures, Structural Dynamics and Materials Conference, Colorado: Denver, April 4–7.

Montesano, J., Fawaz, Z., Poon, C., Behdinan, K., 2014. A microscopic investigation of failure mechanisms in a triaxially braided polyimide composite at room and elevated temperatures. Mater. Des. 53 (1), 1026–1036.

Kueh, A.B.H., Soykasap, O., Pellegrino, S., 2005. Thermo-mechanical behaviour of single-ply triaxial weave carbon fibre reinforced plastic. European Conference on Spacecraft Structures, Materials and Testing, Netherlands: Noordwijk, May 9–13.

Kuth, A.B.H., Pellegrino, S., 2007. Triaxial Weave Fabric Composites. Department of Engineering, University of Cambridge June 30.

Kuth, A.B.H., 2014. Size-influenced mechanical isotropy of singly-plied triaxially woven fabric composites. Composites Part A 57 (1), 76–87.

Miravete, A., Bielsa, J.M., Chiminelli, A., Cuartero, J., Serrano, S., Tolosana, N., Villoria, R.G., 2006. 3D mesomechanical analysis of three-axial braided composite materials. Compos. Sci. Technol. 66 (15), 2954–2964.

Xu, D.S., Ganesan, R., Hoa, S.V., 2007. Buckling analysis of tri-axial woven fabric composite structures subjected to bi-axial loading. Compos. Struct. 78 (1), 140–152.

El-Hajjar, R.F., Shams, S.S., Kehrl, D.J., 2013. Closed form solutions for predicting the elastic behavior of quasi-isotropic triaxially braided composites. Compos. Struct. 101 (15), 1–8.

Kuth, A.B.H., 2013. Buckling of sandwich columns reinforced by triaxial weave fabric. Int. J. Mech. Sci. 66 (4), 45–54.

Zhao, Q., Hoa, S.V., Ouellette, P., 2004. Progressive failure of triaxial woven fabric (TWF) composites with open holes. Compos. Struct. 65 (3-4), 419–431.

Tsai, K.H., Hwan, C.L., Chen, W.L., Chiu, C.H., 2008. A parallelogram spring model for predicting the effective elastic properties of 2D braided composites. Compos. Struct. 83 (3), 273–283.

Zhang, C., Binienda, K.W., 2014. Numerical analysis of free-edge effect on size-influenced mechanical properties of single-layer triaxially braided composites. Appl. Compos. Mater. 21 (6), 841–859.

Potluri, P., Thammandra, V.S., 2007. Influence of uniaxial and biaxial tension on meso-scale geometry and strain fields in a woven composite. Compos. Struct. 77, 405–418.

Naik, N.K., Tiwari, S.I., Kumar, R.S., 2003. An analytical model for compressive strength of plain weave fabric composites. Compos. Sci. Technol. 63, 609–625.

Zhao, L.J., 2010. Micromechanics Study on Damage and Interlaminar Short Fiber Toughening of Composite Laminates. Northeastern University, China.